Role of transmembrane chloride transporters in the fluid secretion of lacrimal gland duct cells

Eszter Vizvári, M.D.

Ph.D. Thesis

Doctoral School of Clinical Medicine

Supervisor: Edit Tóth-Molnár, M.D., Ph.D.

Department of Ophthalmology,

University of Szeged, Szeged,

Hungary

2017

LIST OF RELATED FULL PAPERS

The thesis is based on the following publications:

I. **Vizvári E**, Katona M, Orvos P, Berczeli O, Facskó A, Rárosi F, Venglovecz V, Rakonczay Z Jr., Hegyi P, Ding C, Tóth-Molnár E. Characterization of Na+-K+-2Cl- cotransporter activity in rabbit lacrimal gland duct cells. *Invest Ophthalmol Vis Sci.*
2016; 57(8): 3828-3856.

IF: 3.303

II. Katona M, **Vizvári E**, Németh L, Facskó A, Venglovecz V, Rakonczay Z Jr, Hegyi P, Tóth-Molnár E. Experimental evidence of fluid secretion of rabbit lacrimal gland duct epithelium. *Invest Ophthalmol Vis Sci.* 2014; 55(7): 4360-4367.

IF: 3.404

Other related publication:

III. Kalász H, Tekes K, Pösténvi Z, **Vizvári E**, Sótonyi P, Szabó D, Tóth-Molnár E. Pharmacokinetics of selegiline in a rabbit model. *Letters in Drug Design and Discovery* 2016; 13(8): 752-756.

IF: 1.17

LIST OF ABBREVIATIONS

AE	anion exchanger (Cl^-/HCO_3^- exchanger)
ANOVA	analysis of variance
BCECF-AM	2.7-bis-(2-carboxyethyl)-5-(and-6-)carboxyfluorescein-acetoxymethyl ester
cAMP	cyclic adenosine monophosphate
CA	carbonic anhydrase
CF	cystic fibrosis
CFTR	cystic fibrosis transmembrane conductance regulator
DMEM	Dulbecco modified Eagle medium
FCS	fetal calf serum
H&E	haematoxilin & eosin staining
HEPES	4-(2-hydroxyethyl)-1-piperazineethanesulfonic acid
HPRT	hypoxanthine phosphoribosyl transferase
KO	knockout
LG	lacrimal gland
NKCC	Na^+-K^+-$2Cl^-$ cotransporter
PEG	polyethylene glycol
PFA	paraformaldehyde
PKC	protein kinase C
PMA	phorbol-12-myristate-13-acetate
ROI	region of interest
RT-PCR	real-time reverse transcription polymerase chain reaction
SEM	standard error of the mean
TBS	tris-buffered saline
VIP	vasoactive intestinal peptide
WT	wild type
8-bromo cAMP	8-bromoadenosine-3-5-cyclic monophosphate

1. INTRODUCTION

1.1. Physiology of preocular tear film

Preocular tear film is an essential protector of the ocular surface (1). It is secreted by the lacrimal functional unit which is composed of the ocular surface tissues, lacrimal glands, and their interconnecting sensory and autonomic innervation. This functional unit ensures the stability of the tear film which is essential for the health of ocular surface. Dysfunction of this unit may result in dry eye which is the most common ophthalmic medical problem. Tear film serves multiple functions: 1) maintains the health of corneal and conjunctival surface; 2) protects the anterior surface of the eye from noxious influences; 3) repairs small damages; and 4) creates smooth optical surface for the cornea to subserve clear vision. Tear secretion is a complex process with the involvement of the main and accessory LGs, corneal and conjunctival epithelial cells and Meibomian glands. Tear film is made up of three layers: lipid, water and mucin layers. Lipid layer is formed by the secretions of Meibomian, Zeiss and Moll glands and it is the outermost layer of the tear film. This layer contains low and high polarity of lipids and prevents evaporation and overflow of the tear fluid. The intermediate water layer is formed by the main and accessory lacrimal glands and constitutes the bulk of the tear film. The aqueous layer comprises inorganic salts, glucose, urea, enzymes, proteins, glycoproteins, provides oxygen to the corneal epithelium, washes away debris and foreign particles and contains antibacterial lysozyme. The inner mucin layer is secreted mainly but not exclusively by the conjunctival goblet cells and plays a vital role in the stability of the tear film. The mucin layer lubricates the ocular and palpebral surface and serves to protect the cornea and conjunctiva against the abrasive effects during the blink (2, 3).

1.2. Physiology of lacrimal gland function

Our knowledge about the function of LG is far from complete and therefore more detailed understanding of the physiology and pathophysiology of the LG is essential. Fluid component of tear film is produced predominantly in the exocrine tubuloacinar LGs. LG consists of three main types of cells: acinar, ductal, and myoepithelial cells (4-6). Acinar cell

is the predominant cell type giving approximately 80% of all cells in the gland. These cells form the secretory unit of the gland termed as acinus. Ductal cells make up 15% of all cells in LG forming the duct system and modify the secretory product as it moves through the ducts. Myoepithelial cells are basket-shaped cells that surround the acinar cells and help to forward secreta in the ductal tree.

LG secretes water, electrolytes, and protein in response to different neural and hormonal stimulatory factors. Tear proteins consist of - among other components - lactoferrin, antimicrobial molecules and secretory IgA. Nowadays more than five dozens of lacrimal proteins are known to be secreted primarily by the acinar cells (7). LG is innervated by parasympathetic, sympathetic, and sensory nerves. Parasympathetic nerves regulate the gland mainly through the release of acethylcholine and VIP. Acetylcholine activates M3 muscarinic receptors and VIP binds to VIP receptors located in the basolateral membrane of the lacrimal cells. The sympathetic nerves exert their influence on the lacrimal gland through release of norepinephrine (8).

1.3. Role of LG ducts in lacrimal secretion

Several reports have suggested that LG ducts may play a decisive role in tear production, albeit no definite, especially functional evidence has ever been shown. In 1972, Alexander and coworkers were among the first pioneers who proposed the potential role of duct system in LG secretion, by using micropuncture and catheterization technique. They suggested that LG duct system plays an important role by modifying the compositions of the primary LG acinar fluids and determining the final fluids that reaches the ocular surface which has a much higher K^+ and Cl^- composition compared to the primary fluids (9). These data appeared to suggest that tears are formed in two distinct stages: the plasma-like primary fluid formed by acinar cells is modified by ductal cells during its transit in the ductal lumen. In another ground-breaking publication in 1981, Dartt and colleagues found high Na^+/K^+ ATP-ase density in LG ductal cells by using auto-radiographic method, which was further supported by electron microscopic studies. Secretory vesicles were demonstrated in ductal cells suggesting their role is not limited to ion and water regulation, but also in protein

secretion (10). However, the role of LG duct epithelium on fluid, electrolyte, and protein secretion is not well understood.

Two new methods have been published to study LG duct epithelium during the past decade. Ubels and colleagues introduced the laser capture microdissection technique in LG research to perform gene expression studies on collected duct cells from frozen rat LG sections (11). Numerous genes coding basolateral-to-apical K^+ secretion-related transport proteins were found to be highly expressed in duct cells compared to acinar cells. Another experimental technique - which is the first method allowing functional studying of LG ducts - was described by our laboratory (12). The new isolation technique results in viable duct segments suitable for functional studies. Role and regulation of various ion transporters in lacrimal duct can be studied with the use of these isolated, short-term cultured duct segments.

With the use of isolated duct segments, we started to investigate LG duct functions in the last few years. In a recently published paper by our laboratory, video-microscopic technique was adapted and was used for the first time in lacrimal duct research to investigate fluid secretion of isolated LG duct segments (13). This technique was originally developed by Fernandez-Salazar et al. for the measurement of fluid secretion of pancreatic ducts (14). Accumulating experimental evidences strongly support the hypothesis that the duct system is actively involved in lacrimal fluid secretion. In our video-microscopic fluid secretion experiments, fluid secretion was almost unaffected by inhibition of basolateral HCO_3^- transporters whereas was completely abolished, when basolateral Cl^- uptake was blocked with bumetanide, suggesting the predominant role of Cl^- transport mechanisms over HCO_3^- secreting processes in lacrimal duct fluid secretion in rabbit (13). As bumetanide is a well-known inhibitor of NKCC1, which is located on the basolateral membrane of LG duct cells, this transport mechanism appears to be the main route of cellular Cl^- uptake. Our findings - based on indirect evidences - strongly suggested the importance of CFTR in ductal fluid secretion in rabbit, as forskolin - a well-known activator of CFTR via the elevation of cytosolic cAMP levels – resulted in a significant swelling response in our experimental set-up. Our earlier results suggested the pivotal role of NKCC1 in basolateral Cl^- uptake and the key function of CFTR on the apical membrane in intraluminal Cl^- secretion. Since our knowledge about the role of NKCC1 and CFTR in ductal secretion is limited, further

investigations have been initiated to study the role of these transporters in the secretory processes of LG ducts.

There are limited reports about the role of NKCC1 in lacrimal gland secretion**.** Existence of a furosemide sensitive secretory mechanism in rabbit LG was proved by Dartt and colleagues (10). Their work provided indirect evidence that coupled transport of Na^+ and Cl^- is important in LG fluid secretion. Experimental evidence was found for expression of NKCC1 on the basolateral membranes of LG duct cells of rat, rabbit and mouse (11, 15, 16). Walcott et al. demonstrated the presence of NKCC1 in duct and acinar cells of mice LG (16). Important role of NKCC1 in fluid secretion by the LG of mice was also proved. Mouse LGs were investigated *in situ* and data were obtained from the entire LG. However, apart from our secretory results there is no available data about the role and function of NKCC1 in LG duct epithelium.

Important role of CFTR has been widely demonstrated in the maintenance of homeostasis in different secretory epithelia including pancreas, salivary glands, sweat glands and airways epithelium (17-22). Furthermore, there are several clinical data about dry eye disease with various severity seen in CF patients, which further strengthens the potential influence of CFTR in altered tear secretion (23-25). Despite of these clinical observations role of CFTR in production of preocular tear film is only partially investigated and its functional involvement in LG secretion is unknown. Accumulating evidences from rat and rabbit LG gene expression studies demonstrated the predominant expression of CFTR in LG duct cells (11, 15, 26). These studies were mostly descriptive without exploring the functional aspect of CFTR in LG secretion. In our earlier work with rabbit lacrimal duct segments, we were unable to carry out direct investigation of the apically located CFTR since the luminal space cannot be reached in the isolated, fragile, small sealed ducts (13). Availability of transgenic mouse models carrying genetic defects in CFTR allows the direct examination of the role of CFTR (27-29). Presently we conducted the first study in lacrimal gland research which focuses on the functional role of CFTR in LG secretion with the use of CFTR transgenic mouse model.

2. AIMS OF THE STUDY

Previous studies of our laboratory have shown that isolated duct segment from rabbit LG was able to secrete fluid into the luminal space in response to cAMP-elevator forskolin, which was completely blocked by bumetanide (13). As bumetanide is a well-known inhibitor of NKCC1 located on the basolateral membrane, this blockage suggested the important role of NKCC1. Role of CFTR was also suggested, since elevation of cytosolic cAMP is tend to activate CFTR on the apical membrane.

Therefore aims of our experiments were:

1) to investigate the functional role and the activity profile of NKCC1 in isolated LG ducts.

2) to determine the role of CFTR in tear secretion and in the maintenance of ocular surface integrity as well as the presence and function of CFTR in LG ductal secretion using LG ducts isolated from wild type (WT) and CFTR knockout (KO) animals.

3. MATERIALS AND METHODS

3.1. Animals

Rabbits

Adult male New Zealand white rabbits weighing 2-2.5 kg were used (source of animals: Devai Farm, Kondoros, Hungary). All animals were kept at a constant room temperature of 22 °C, under 12-h light and dark cycles, and were allowed free access to water and standard laboratory chow. The animals were narcotized with a mixture of ketamine (10 mg/kg, intravenously) and xylazine (3 mg/kg, intravenously) and were euthanized with pentobarbital overdose (80 mg/kg, intravenously). The intraorbital lacrimal glands were carefully dissected (following a wide temporal canthotomy and conjunctival incision the eyeball was dislocated inferonasaly and the lacrimal gland revealed under the roof of the orbit).

Mice

CFTR KO mice were originally generated by Ratcliff et al. and was a kind gift of Ursula Seidler (27, 28). The mice were congenic on the FVB/N background. No wild-type CFTR protein is made by the null CF mice, since the hypoxanthine phosphoribosyl transferase (HPRT) cassette disrupts the *cftr* coding sequence and introduces a termination codon. None of the possible RNA transcripts from the disrupted locus can encode a functional CFTR protein. Genotyping was performed by RT-PCR. The animals were kept at a constant room temperature of 24°C with a 12 h light–dark cycle and were allowed free access to specific CFTR chow and drinking solution in the Animal Facility of the First Department of Medicine, University of Szeged. The mice received electrolyte drinking solution containing polyethylene glycol (PEG) and high HCO_3^- (in mM: 40 Na_2SO_4, 75 $NaHCO_3$, 10 NaCl, 10 KCl, 23 g l^{-1} PEG 4000), and a fiber-free diet (Altromin, C1013) to allow survival beyond weaning. All mice were genotyped prior to the experiments. Wild type (WT) refers to the +/+ littermates of the CFTR KO mice. The mice used in this study were 8-24 weeks old and weighted 14-24, gender ratio was 1:1 for all groups.

All experiments were conducted in compliance with the ARVO Statement for the Use of Animals in Ophthalmic and Vision Research. The protocol has been approved by the Ethical Committee for the Protection of Animals in Research of the University of Szeged, Szeged, Hungary and conformed to the Directive 2010/63/EU of the European Parliament.

3.2. Solutions and chemicals

Isolation solution contained DMEM supplemented with 100 U/ml collagenase (Worthington Lakewood, NJ, USA) and 1 mg/ml bovine serum albumin. Storage solution contained DMEM and 3% (wt/vol) bovine serum albumin. Culture solution contained McCoy's 5A tissue culture medium, 10% (vol/vol) fetal calf serum, and 2 mM glutamine. Media supplements (DMEM, McCoy, fetal calf serum, glutamine and bovine serum albumin) were purchased from Sigma-Aldrich (Budapest, Hungary). Composition of solutions used for superfusion of isolated ducts during NKCC1 activity measurements is summarized in Table 1. All chemicals listed in Table 1 were purchased form Sigma-Aldrich (Budapest, Hungary).

Carbachol (carbamoylcholine chloride), forskolin, bumetanide, PMA, calcium ionophore A23187, 8-bromoadenosine-3-5-cyclic monophosphate (8-bromo cAMP), and VIP were purchased from Sigma-Aldrich (Budapest, Hungary). BCECF-AM was purchased from Invitrogen (Thermo Fisher Scientific, Waltham, Massachusetts, USA).

Table 1. Solutions and their compositions used for the measurement of NKCC1 activity.

Compound	Content of solution (mM)									
	A	B	C	D	E	F	G	H	I	J
NaCl		100	40	40			140	100		
KCl			60							
HEPES	10	10	10	10	10	10	10	10	10	10
K_2HPO_4	0.8	0.8	0.8	0.8	0.8	0.8	0.8	0.8	0.8	0.8
KH_2PO_4	0.2	0.2	0.2	0.2	0.2	0.2	0.2	0.2	0.2	0.2
$MgCl_2$	1	1	1	1	1	1	1	1		
$CaCl_2$	1	1	1	1	1	1	1	1		
TMA-Cl	140			60	100					
NMG						140				
NH_4Cl		40	40	40	40			40		
Glucose	5	5	5	5	5	5	5	5	5	5
Magnesium gluconate									1	1
Calcium-gluconate									1	1
Sodium-gluconate									140	100
Ammonium-sulphate										40

3.3. Measurement of tear secretion and corneal fluorescein staining

Tear production was measured in anesthetized mice using phenol red impregnated cotton threads (Zone-Quick, Showa Yakuhin Kako Ltd, Japan) applied into the lateral canthus of both eyes for 5 minutes. Color of the threads turns red in contact with the tears. Wetting length was measured in millimeters under a dissecting microscope.

Ocular surface integrity was evaluated by applying 0.5 μL of 5% fluorescein sodium into the conjunctival sac, followed by slit-lamp biomicroscopy (Inami L0198, Tokyo, Japan) through cobalt-blue filter. Images were captured with an anterior segment digital camera (Inami L-0541DC, Tokyo, Japan) attached to the slit-lamp. Staining was assessed by using the NEI grading system (30). To quantify the staining changes, corneas were divided into five regions and staining was assessed and rated in each region from 0 to 3. Total scores from the five regions were recorded.

3.4. H&E staining

Freshly dissected LG tissues, from both WT and KO mice, were fixed in 4% buffered formaldehyde and embedded in paraffin, then 3.5 µm thin serial sections were cut and stained with H&E.

3.5. Immunofluorescence

Fifteen µm thick cryostat sections were rehydrated by washing in tris-buffered saline (TBS, 20 mM Tris-HCl pH: 7.5, 150 mM NaCl) for 5 minutes, then fixed in 2% PFA. After washing the sections in TBS three times for 5 minutes each, the samples were permeabilized with 0,1% Triton-X in TBS for 10-15 minutes. The sections were blocked with 5% FCS in TBS for 1 hour at room temperature followed by an overnight incubation with primary antibodies. The next day the samples were incubated with secondary antibody for 1 hour and Hoechst (1:1000, Sigma) for 20 minutes at room temperature.

Primary antibodies used for NKCC1 staining were purchased from Santa Cruz Biotechnology (goat polyclonal, N-16, Santa Cruz, CA), with the dilution being 1:50. Secondary antibodies used was fluorescein isothiocyanate (FITC)-conjugated AffiniPure donkey anti-goat IgG (Jackson ImmunoResearch Laboratories, West Grove, PA), at a dilution of 1:200. Rhodamine-conjugated phalloidin, at a dilution of 1:200, was used to stain F-actin to show the morphological profiles of LG.

Primary antibodies for CFTR (1:100) were purchased from Alomone Labs, Jerusalem, Israel, secondary antibody, Alexa-488 conjugated goat anti-rabbit (1:1000) was obtained from Abcam (Cambridge, UK). The samples were examined under a Zeiss LSM 880 confocal laser scanning microscope (Oberkochen, Germany). Images were analyzed with LSM image browser and PhotoShop (Adobe Systems, Mountain View, CA).

3.6. Isolation and culture of lacrimal duct segments

Rabbit LG interlobular ducts were isolated as previously described by our laboratory (12). Briefly, LGs were dissected and transferred to a sterile small flat-bottom glass flask containing a cold (+4 ^{o}C) storage solution. Isolation solution was injected into the

interstitium of the glands and the tissue pieces were transferred to a glass flask containing 2 ml of isolation solution for incubation in a shaking water bath at 37 ^{O}C. Isolation solution was removed after incubating for 25 min and 5 ml of fresh cold storage (+4 ^{O}C) solution was added to the flask. LG tissue samples were transferred to a glass microscope slide and viewed under stereo microscope. Inter-, and intralobular ducts were micro-dissected and after microdissection, intact LG ducts were transferred to the culture solution in a Petri dish. Ducts were cultured overnight in a 37 ^{O}C incubator gassed with 5 % CO_2.

3.7. Intracellular pH measurement with fluorophotometry

After overnight culture, LG duct segments were carefully transferred to a coverslip (24 mm) pre-treated with diluted (dilution ratio 1:9) poly-l-lysine (Sigma-Aldrich). The coverslip formed the base of a perfusion chamber mounted on an inverted microscope (Olympus, Olympus Ltd, Budapest, Hungary). Ducts were bathed in standard HEPES solution at 37°C and loaded with the pH-sensitive fluorescent dye BCECF-AM (2 µM) for 25 minutes. Thereafter, the ducts were continuously superfused with solutions at a rate of 4 to 5 ml/min. Intracellular pH was measured using an imaging system (Cell; Olympus, Olympus Ltd, Budapest, Hungary). Four to six ROIs of 5 to 10 cells each in an intact duct were excited at 490 nm and 440 nm, respectively, and the 490/440 fluorescence emission ratio was then measured at 535 nm. One intracellular pH measurement per second was recorded.

3.8. Measurement of NKCC1 activity

Ammonium pulse technique was used to measure the activity rate of NKCC1 by determining the rate of intracellular acidification caused by NH_4^+ entry into the cells via this transport mechanism on abrupt application of NH_4Cl as described by Shumaker et al. and Heitzmann et al (31, 32). The theoretical background of the method is the competition between NH_4^+ and K^+ uptake as NKCC1 can accept NH_4^+ at its K^+ binding site. The fluorescence ratio of BCECF-loaded lacrimal duct epithelial cells was measured as a function of time. An increase in fluorescence ratio corresponds to the elevation of intracellular pH.

The addition of NH_4Cl resulted in a four-phase curve representing the four-phasic alterations in cytosolic pH: 1) rapid initial alkalinization caused by NH_3 entry into the cell followed by 2) a slower decline in pH representing NH_4^+ uptake of the cell via – among other potentially contributing channels - NKCC1. The third phase of cytosolic pH alteration is a rapid acidification after stoppage of NH_4Cl administration followed by the 4th phase representing a pH recovery determined by proton extrusion and HCO_3^- import. The kinetics of the 2nd phase acidification is of particular interest in relation to NKCC1 activity, as this phase is associated with influx of NH_4^+, a substrate for the co-transporter. NKCC1 activity was therefore determined as bumetanide-sensitive part of the 2nd phase acidification representing bumetanide dependent NH_4^+ entry into the cell. The slope of the 2nd phase acidification was characterized by calculating the initial rates of recovery from alkalosis (dpH/dt) over the first 60 seconds.

3.9. Measurement of fluid secretion of LG ducts

Videomicroscopic technique was used for measurement of ductal fluid secretion (13, 14). Fluid secretion into closed intraluminal space of cultured lacrimal gland interlobular ducts was analyzed using the swelling method. Cultured lacrimal gland duct segments were carefully transferred to a coverslip pre-treated with Cell-Tak. The coverslip formed the base of a perfusion chamber mounted on an inverted microscope (Olympus Ltd., Budapest, Hungary). The chamber was perfused with solutions via an infusion pump at approximately 2.5 ml/min. The temperature of perfusion chamber was maintained at 37 °C. Ducts were visualized at high magnification (40 x objective). Bright-field images were acquired at set time intervals (5 sec in case of osmotic permeability measurements and 1 min in case of ductal fluid secretion experiments) using a charge-coupled device camera coupled to a computer. Both the duration of experiments and the time intervals between images were defined in Image J software. An image series in TIFF-format was generated containing all of the images collected from the same experiment. Scion Image (Scion Corporation, Frederick, MD, USA) software was used to analyze changes to obtain values from the area corresponding to the luminal space in each image.

The initial lumen length (L_0) and the lumen area (A_0) were measured directly from the pixel intensities on the first image. The lumen diameter was calculated assuming cylindrical setup of the duct, from the formula $2R=A_0/l_0$. The luminal surface area was calculated as $2\pi R_0 L_0$, also assuming cylindrical geometry. Measurements from subsequent individual images were normalized to the first lumen area in the series (A_0) thus giving values for the relative area ($A_R=A/A_0$). Relative luminal volume ($V_R=V/V_0$) of the ducts was then calculated from the relative image area. These calculations were done using Scion Image and Microsoft Excel software.

In fluid secretion measurements, forskolin was added to the perfusate after 10 min of superfusion with HEPES-buffered or HCO_3^-/CO_2-buffered solution. At the end of each experiment, perfusion was changed to hypotonic solution for 5 min in order to confirm epithelial integrity. Complete sealing was proved by rapid swelling as a response to hypotonic challenge. Data obtained from ducts not showing swelling response were discarded.

3.10. Statistical analysis

A mixed ANOVA model was used for the calculation of NKCC1 activity, and also for the calculation of ductal fluid secretion. For the calculation of NKCC1 activity, the effect of “bumetanide” was taken into account as a fixed effect. The effect of the individual “duct” and the "duct and effect of bumetanide" interaction (we assumed that the value of the effect of bumetanide depends on the individual duct) were taken into account as random effects in the model. For the calculation of ductal fluid secretion, effects of the stimulatory compound (forskolin) was taken into account as “fixed effects”. The effect of the individual “duct" and the “duct and effects of forskolin“ interaction were taken into account as random effects in the model. Kruskal-Wallis test with Dunn method was used for the analysis of tear secretion. SPSS 22 statistical software (IBM, New York, USA) was used to analyze the data, which were presented as means ± SEM. A p value of less, than 0.05 was regarded as significant.

4. RESULTS

4.1. BASOLATERAL CHLORIDE TRANSPORT OF LG DUCT CELLS: ROLE OF NKCC1

4.1.1. Localization of NKCC1 in rabbit LG

Immunofluorescence demonstrated presence of NKCC1 on the basolateral membranes of both acinar and ductal cells in rabbit LG, with the intensity being more pronounced in acinar cells (Figure 1).

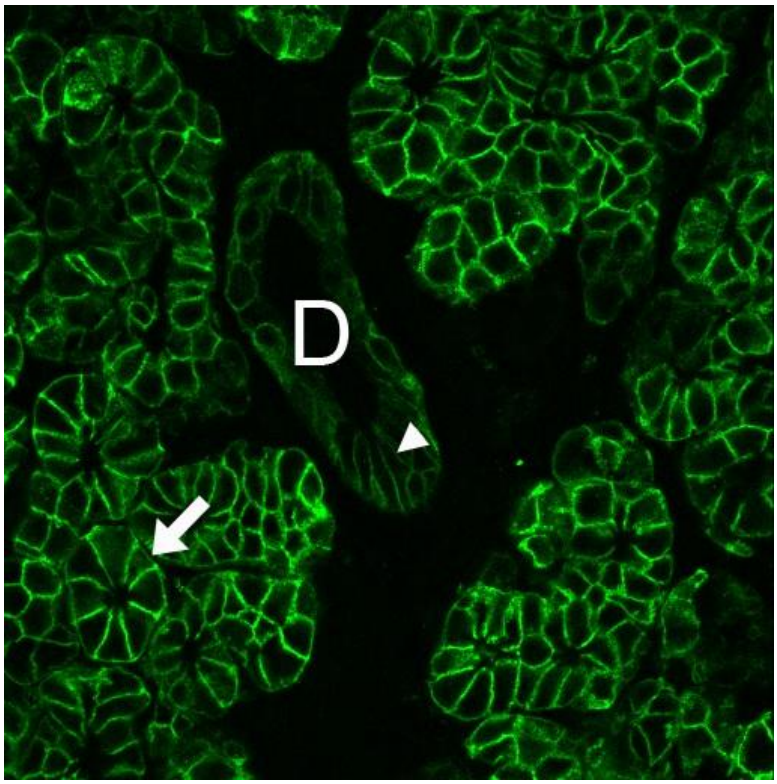

Figure 1. Confocal immunofluorescence image of NKCC1 staining in rabbit LG, demonstrating basolateral immunoreactivity in both acinar (arrow) and ductal cells (arrowhead), especially in the lateral membranes. However, the staining in ducts (D) was considerably weaker than that of acini.

4.1.2. Characterization of NKCC1 activity in rabbit LG ducts

In general, NKCC1 can be characterized functionally during NH_4^+ pulse as bumetanide sensitive, Na^+ and K^+ dependent NH_4^+ enrty into the cells. In the first series of experiments we tested the hypothesis that NKCC1 can transport NH_4^+ instead of K^+ with a resultant change in intracellular pH. Ammonium induced acidification was reduced in the presence of high K^+ concentration in the superfusate (solutions A, C and D, Table 1), indicating competition between K^+ and NH_4^+ ((low K^+, 0.027±0.002 pH unit/60 seconds; high K^+, 0.014±0.002 pH unit/60 seconds; p=0.008; Figure 2A). To determine whether NH_4^+ transport in duct cells occurs via a Na^+-dependent pathway, the NH_4^+ pulse was repeated with tetramethylammonium-chloride instead of NaCl in the superfusate (solutions A, B and E, Table 1). Ammonium-induced cell acidification was reduced significantly in the absence of Na^+ (Na^+, 0.034±0.002 pH unit/60 seconds; Na^+ free, 0.021±0.002 pH unit/60 seconds; p= 0.012; Figure 2B). To test the existence of a bumetanide-sensitive basolateral transport system (indicative for the presence of NKCC1), standard NH_4^+ pulse was administered in the presence and absence of bumetanide (solutions A and B, Table 1). In the presence of bumetanide (100µM), NH_4^+- induced cell acidification was significantly reduced in duct cells (control, 0.029±0.002 pH unit/60 seconds; bumetanide, 0.018±0.002 pH unit/60 seconds; p= 0.004, Figure 2C). These results confirm the existence of a Na^+ dependent, bumetanid-sensitive pathway in the duct cells where K^+ transport is in competition with NH_4^+ suggesting the functional involvement of NKCC1.

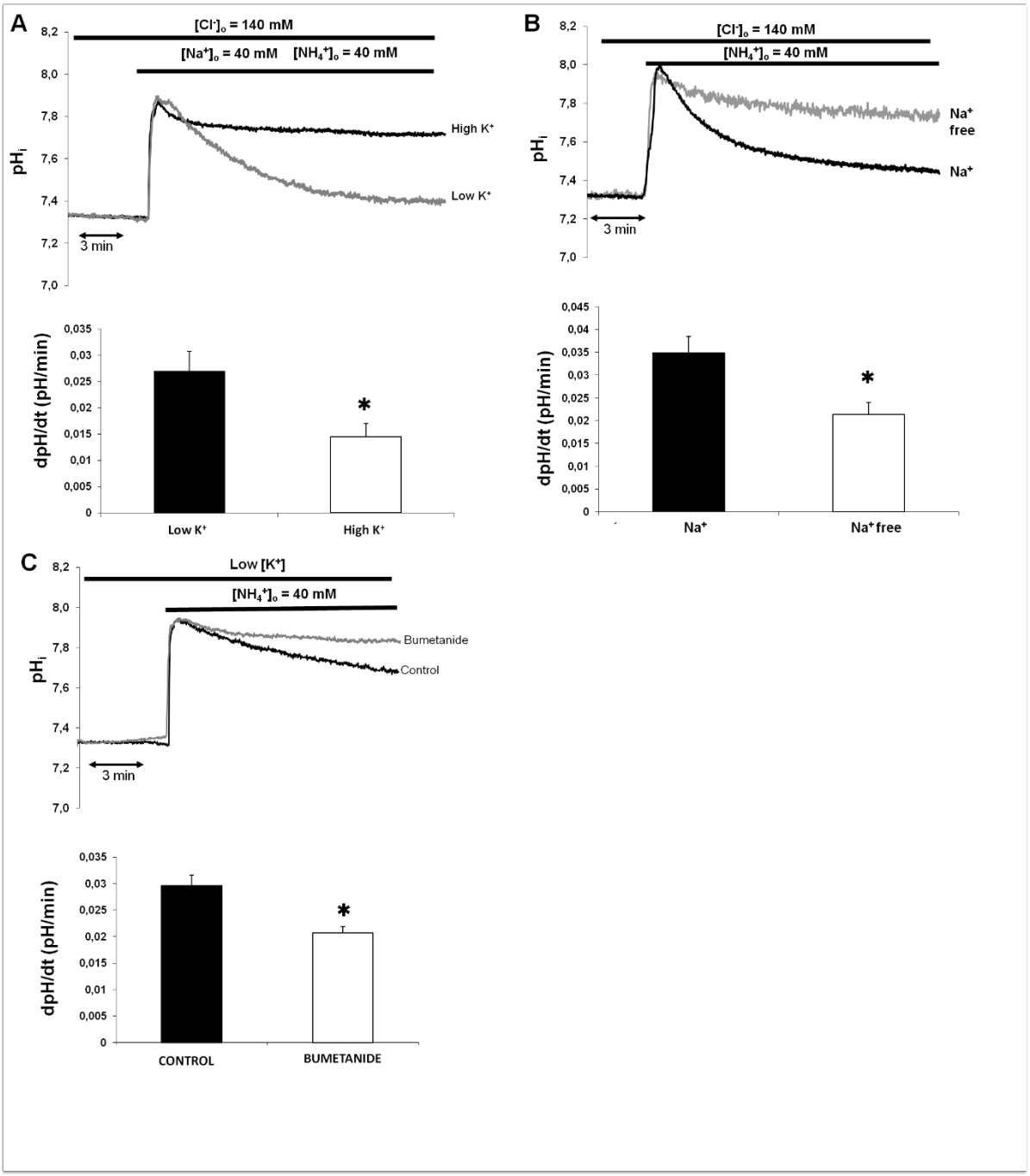

Figure 2. Functional presence of NKCC1 in isolated rabbit LG ducts. A: NH_4^- induced acidification during ammonium pulse is completely blocked by high K^+ content of the medium indicating competition between NH_4^+ and K^+ transport. B: NH_4^+ transport process is Na^+ dependent. C: NH_4^+ transport is completely blocked by the administration of bumetanide. For each panel (A, B, C): top: representative curves of the experiments; bottom: initial rate of recovery from alkalosis (dpH/dt) over the first 60 seconds. Data was obtained from six ducts isolated from three different animals in each series,*$p<0.05$.

4.1.3. Influence of repeated $NH4^+$ pulse on the slope of second phase acidification

To determine whether repeated ammonium pulse administration itself could influence the slope of the second phase, three consecutive pulses were added to the same duct segment (solutions G and H, Table). The slope of the second phase was stable during repeated pulses; thus, the ‘‘fatigue’’ effect of the repeated base administration should not be taken into consideration during calculation of NKCC1 activity (pulse 1, 0.08±0.006 pH unit/60 seconds; pulse 2, 0.08±0.005 pH unit/60 seconds; pulse 3, 0.078±0.006 pH unit/60 seconds; Figure 3).

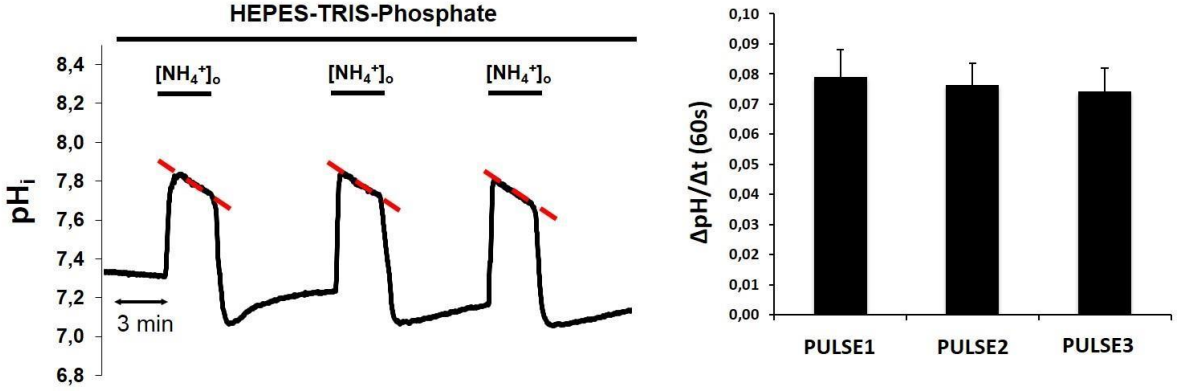

Figure 3. Role of repeated ammonium pulse on the slope of second phase acidification. Ducts were superfused with HEPES-buffered solution and 3 consecutive ammonium pulses were administered. **Left panel)** representative curves of the experiments. **Right panel)** summary of data from left panel. Initial rate of recovery from alkalosis (dpH/dt) over the first 60 seconds is shown. Data was obtained from six ducts isolated from three different animals.

4.1.4. Basal activity of NKCC1

To determine whether basal activity of NKCC1 affects the measurements, the slope of second phase acidification was determined and compared during $NH4^+$ pulse in the presence and absence of bumetanide (solutions G and H, Table). Basal activity of NKCC1 was negligible and statistically not significant (0.009±0.006 pH unit/60 seconds; p=0.320; Figure 4).

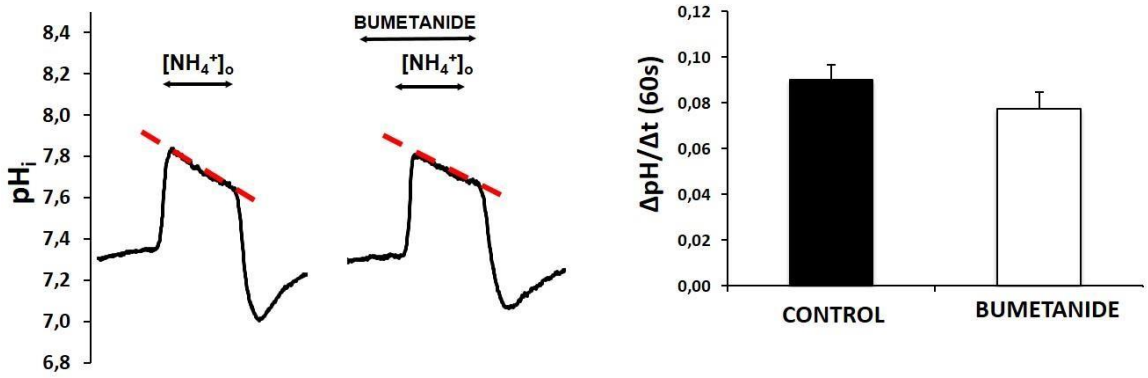

Figure 4. Basal activity of NKCC1. Ducts were superfused with HEPES-buffered solution and ammonium pulse was administered in the absence and presence of bumetanide (100 µM). Initial uptake rate of NH_4^+ was calculated and compared. **Left panel)** representative curves of the experiments. **Right panel)** summary of data from left panel. Initial rate of recovery from alkalosis (dpH/dt) over the first 60 seconds is shown. Data was obtained from six ducts isolated from three different animals.

4.1.5. Activation of NKCC1 by low cytosolic Cl^-

Isolated LG duct segments were preincubated in Cl^- -free solution for 20 minutes, then $NH4^+$ pulse was performed in the presence and absence of bumetanide in these experiments (solutions I and J, Table). The results are summarized in Figure 5. The bumetanide-inhibited component of the second-phase pH alteration during ammonium pulse represents the activation of NKCC1 by low cytosolic Cl^-. Low cytosolic Cl^- increased the activity of NKCC1, the increase was statistically significant (0.026±0.009 pH unit/60 seconds; p=0.023).

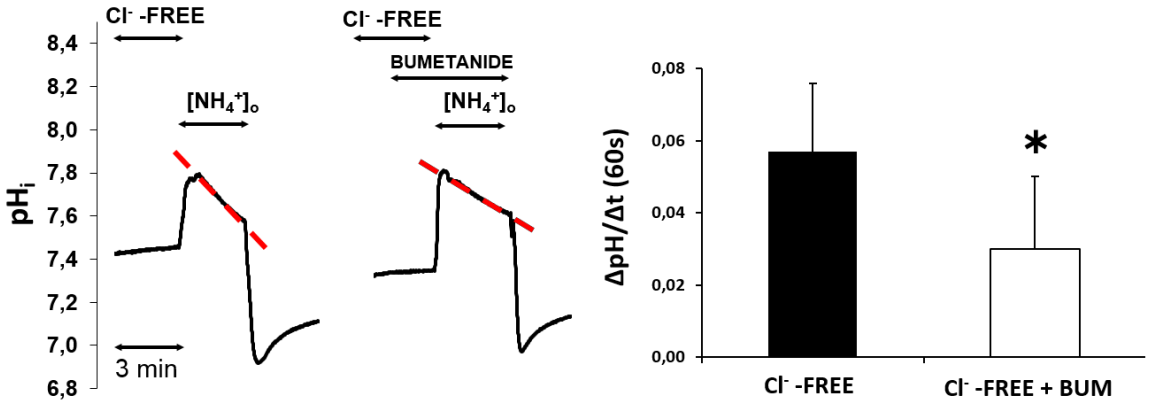

Figure 5. The effects of low cytosolic Cl^- concentration on NKCC1 activity. Ducts were superfused with Cl^- free medium and ammonium pulse was administered in the absence and presence of bumetanide (bum, 100 µM). Initial uptake rate of NH_4^+ was calculated and compared. **Left panel)** representative curves from our experiments. **Right panel)** summary of data from left panel. Initial rate of recovery from alkalosis (dpH/dt) over the first 60 seconds is shown. Data was obtained from nine ducts isolated from four different animals. *: $p<0.05$.

4.1.6. Activation of NKCC1 by hyperosmolarity

To investigate the role of hyperosmotic environment in the activation of NKCC1, ducts were preincubated with bath solution of 390 mOsm/l in the absence and presence of bumetanide (solution G+100 mM mannitol and solution H, Table 1). Hyperosmotic challenge, that is elevation of bath osmolarity from 290 mOsm to 390 mOsm increased the activity of NKCC1 significantly (0.024±0.007 pH unit/60 seconds, $p=0.025$) indicating that hyperosmolarity has an important role in the activation of NKCC1. The results are summarized in Figure 6.

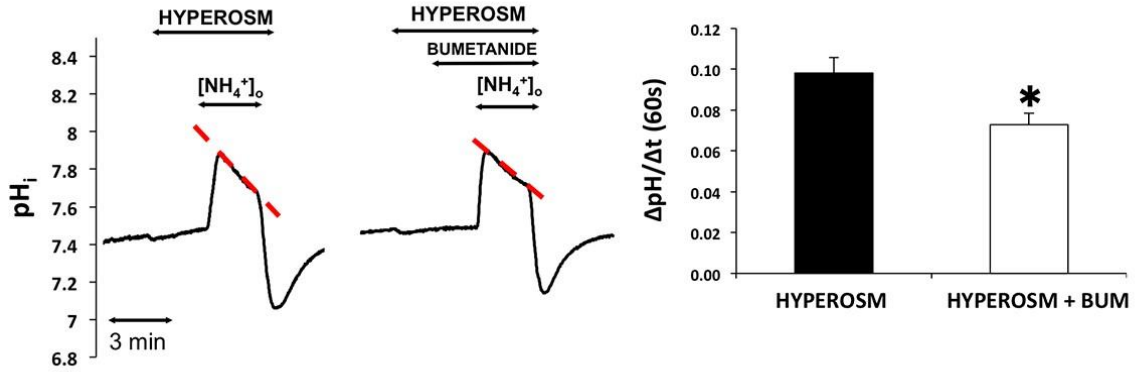

Figure 6. Effect of hyperosmolarity on NKCC1 activity. Ducts were superfused with hyperosmotic medium (390 mOsm) and ammonium pulse was administered in the absence and presence of bumetanide (bum). Initial uptake rate of $NH_4^+$was calculated and compared. Hyperosmotic challenge enhanced the activity of NKCC1. **Left panel)** representative curves of the experiments. Summary of data is shown at the **right panel)** initial rate of recovery from alkalosis (dpH/dt) over the first 60 seconds is shown. Data was obtained from five ducts isolated from three different animals. *: $p<0.05$.

4.1.7. Effects of carbachol, PMA, and Ca^{2+} ionophore A23187 in the activation of NKCC1

Acetylcholine analogue carbachol was used to investigate the effect of cholinergic agonists in the activation of NKCC1. Isolated ducts were superfused with HEPES-buffered solution and $NH4^+$ pulse was administered in the absence and presence of bumetanide after preincubation with carbachol (100 µM, 5 minutes, solutions G and H, Table 1). Results are summarized in Figure 7A. The slope of second-phase acidification was increased compared to the control as a result of cholinergic stimulation. Bumetanide treatment (100 µM) did not change the slope of second phase acidification during NH^{4+} pulse, indicating that carbachol had no significant effect on NKCC1 activity (0.006±0.006 pH unit/60 seconds; $p=0.388$). To further elucidate the role of cholinergic cellular signaling pathways in the activation of NKCC1 in rabbit LG ducts, the effects of Ca^{2+} ionophore A23187 and protein kinase C (PKC) activator PMA was investigated. Preincubation with Ca^{2+} ionophore A23187 (3 min, 1 µM) was followed by $NH4^+$ pulse administration with and without bumetanide in the

superfusate. Calcium ionophore A23187 did not result in activation of the cotransporter (0.002±0.002 pH unit/60 seconds; p=0.226, Figure 7B). In the next series of experiments, effect of PMA was tested. Ammonium pulse was administered to the ducts in the absence and presence of bumetanide after preincubation with PMA (3 minutes, 100 nM, solutions G and H, Table). Bumetanide treatment slightly but significantly reduced the slope of second phase acidification (0.011 ± 0.001 pH unit/60 seconds; p= 0.0007, Figure 7C).

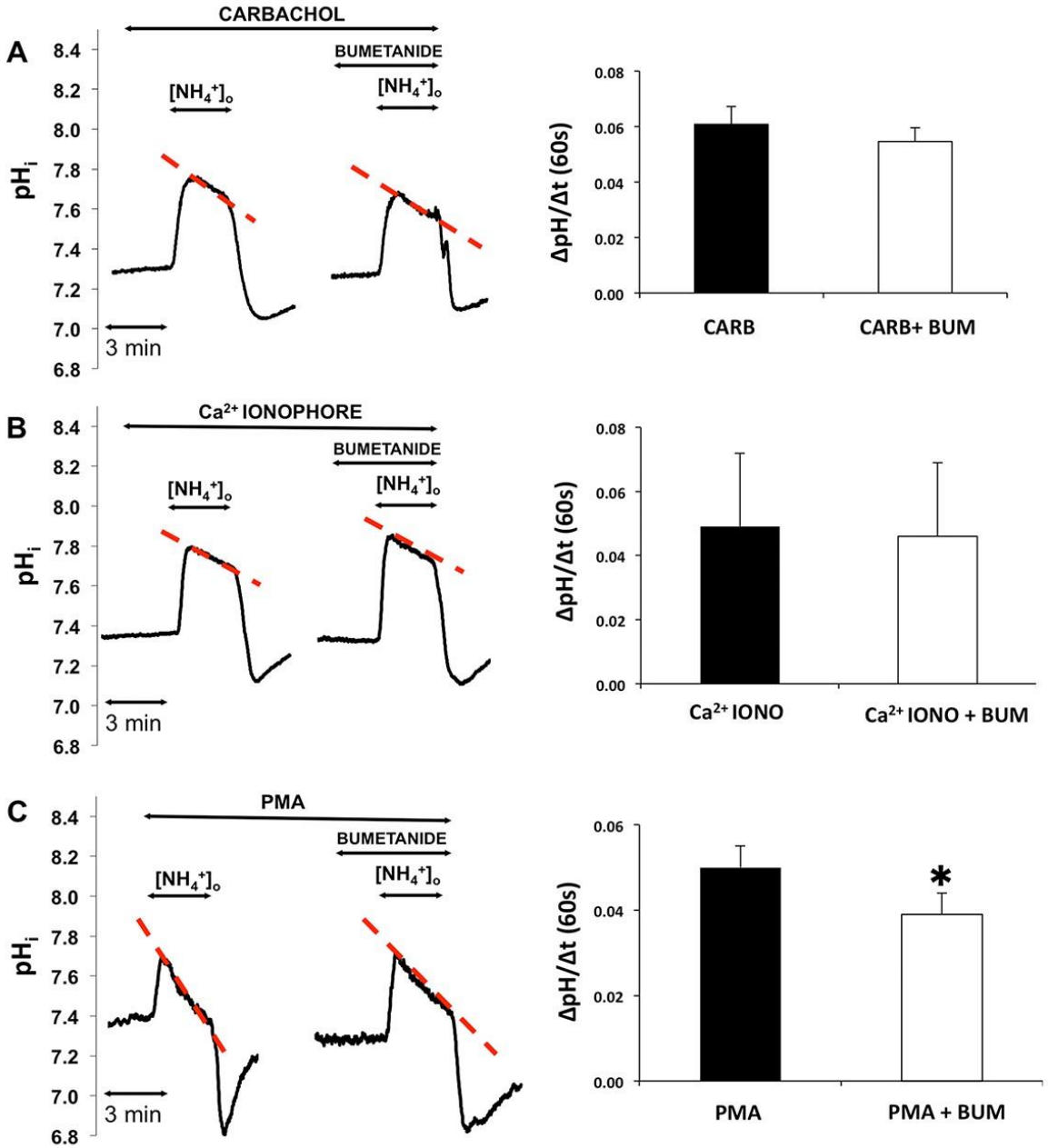

Figure 7. Effect of cholinergic signaling pathway on NKCC1 activity. Ducts were superfused either with **A)** carbachol (carb, 100 µM); or **B)** Ca^{2+} ionophore A23187 (iono, 1µM) or **C)** PMA (100 nM) and ammonium pulse was administered in the absence and presence of bumetanide (bum, 100 µM). Initial uptake rate of $NH_4^+$was calculated and compared. **Left panels)** representative curves of the experiments. Summary of data is shown at the **right panels)** initial rate of recovery from alkalosis (dpH/dt) over the first 60 seconds is shown. Data was obtained from seven ducts isolated from three different animals in each group of experiments.*: $p<0.05$

4.1.8. Activation of NKCC1 by VIP

Parasympathetic nerves release VIP in addition to the cholinergic agonist acetylcholine; thus, in the next series of experiments we investigated the effect of VIP in the activation of NKCC1. Isolated ducts were superfused with HEPES-buffered solution and $NH4^+$ pulse then was administered in the absence and presence of bumetanide after preincubation with VIP (5 minutes, 200 nM, solutions G and H, Table). The results are summarized in Figure 8. VIP treatment increased the rate of second phase acidification, which was reduced by bumetanide (100 µM). The bumetanide-sensitive part of the second phase acidification was 0.051±0.009 pH unit/60 seconds (p=0.033), indicating the VIP-induced marked increase in NKCC1 activity.

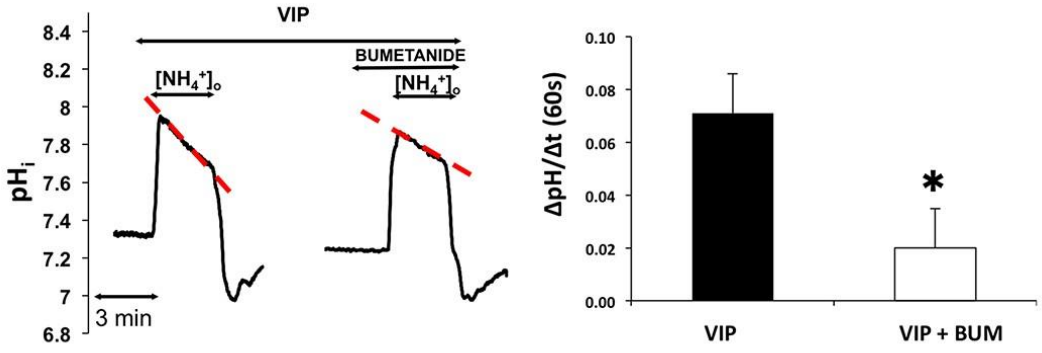

Figure 8. Effect of VIP on NKCC1 activity. Ducts were superfused with VIP (200 nM) and ammonium pulse was administered in the absence and presence of bumetanide (bum, 100 µM). Initial uptake rate of $NH_4^+$was calculated and compared. **Left panel)** representative

curves of the experiments. Summary of data is shown at the **right panel)** initial rate of recovery from alkalosis (dpH/dt) over the first 60 seconds is shown. Data was obtained from five ducts isolated from three different animals. *: $p<0.05$.

4.1.9. Activation of NKCC1 by forskolin and cell permeable cAMP analogue 8-bromo cAMP

Next, we studied the role of elevated intracellular cAMP level in the activation of NKCC1. Isolated ducts were superfused with HEPES-buffered solution and $NH4^+$ pulse then was administered after a 5-minute incubation with forskolin (10 µM) in the absence and presence of bumetanide (solutions G and H, Table). The results are summarized in Figure 9A. Forskolin increased the rate of second phase acidification, which was reduced by bumetanide (100 µM). The bumetanide-sensitive part of the second phase acidification was 0.024±0.008 pH unit/60 seconds ($p=0.045$), indicating the forskolin-induced significant increase in NKCC1 activity. To further verify the effect of elevated cytosolic cAMP level in the activation of NKCC1, cell permeable cAMP analogue was used. Ammonium pulse was administered in the absence and presence of bumetanide after preincubation with 8-bromo cAMP (100 µM, 5 minutes). The bumetanide-sensitive part of the second phase acidification was 0.044±0.007 pH unit/60 seconds ($p=0.011$), representing a statistically significant increase in NKCC1 activity caused by cell-permeable cAMP analogue 8-bromo cAMP (Figure 9B).

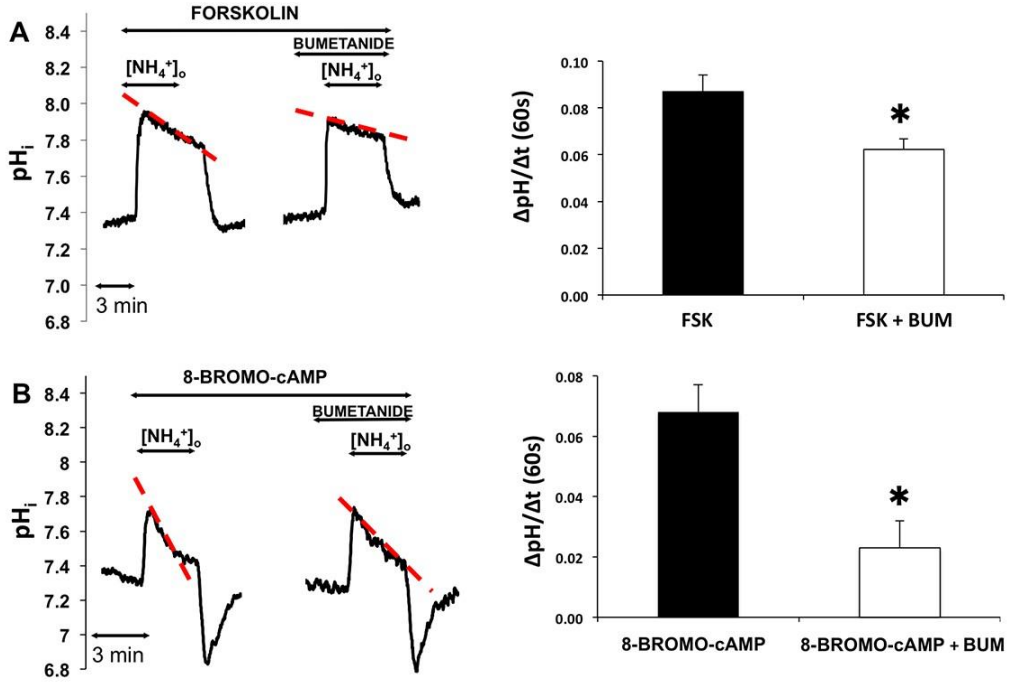

Figure 9. Effects of forskolin and cell permeable cAMP analogue 8-bromo cAMP on NKCC1 activity. Ducts were superfused either with forskolin (FSK, 10 µM, **Figure 9A**) or 8-bromo cAMP (100 µM, **Figure 9B**) and ammonium pulse was administered in the absence and presence of bumetanide (bum, 100 µM). Initial uptake rate of $NH_4^+$was calculated and compared. **Left panels)** representative curves of the experiments. Summary of data is shown at the **right panels)** initial rate of recovery from alkalosis (dpH/dt) over the first 60 seconds is shown. Data was obtained from five ducts isolated from three different animals in both groups of experiments.*: $p<0.05$.

4.2. ROLE OF CFTR-MEDIATED CHLORIDE TRANSPORT IN LACRIMAL SECRETION

4.2.1. Role of CFTR in tear secretion and corneal fluorescein staining using CFTR KO mice

Tear secretion was measured in three age groups in both WT and KO mice, at 8-10 weeks of age, at 14-16 weeks of age and at 20-24 weeks of age. Data from both eyes were averaged and evaluated. Tear secretion of KO animals in all age groups were significantly lower as compared to their WT littermates (8-10 weeks: p=0.0008; 14-16 weeks: p=0.0007; 20-24 weeks: 0.0004). To study the effect of age (or duration of the disease in KO animals)

in tear secretion, results were calculated not only vertically (i.e. separately in different age groups, comparing WT and KO measurements, see above) but also horizontally, with the comparison of tear secretion in different age groups separately in WT and in KO animals. Tear secretion of WT mice measured at the age of 14-16 weeks was significantly higher compared to the 8-10 weeks group ($p=0.006$). However, no significant differences were observed between secretion data at the age of 14-16 weeks and 20-24 weeks ($p=0.957$). We could not find statistically significant differences in tear secretion of KO animals measured in different age groups (8-10 weeks vs. 14-16 weeks: $p=0.075$; 14-16 weeks vs. 20-24 weeks: $p=0.136$). (Figure 10A).

The potential inter-ocular variability of tear secretion was also investigated both in WT and CFTR KO animals in each age group. Inter-ocular difference in tear secretion did not differ either in WT or in CFTR KO mice (Figure 10B).

Fluorescein staining was evaluated in both WT and KO mice at 8-10 weeks of age and at 20-24 weeks of age. Data from both eyes were pooled together. Corneal staining score was 1.0 ± 0.66 in WT mice ($n=6$) and 6.83 ± 1.16 in KO mice ($n=6$, $p=0.0002$) in animals at 8-10 weeks, while in the 20-24 weeks group, the staining was 4.17 ± 0.88 in WT mice ($n=6$) and 11.17 ± 1.16 in KO animals ($n=6$, $p=0.0004$). Corneal staining images of WT and KO mice at 10 weeks and 24 weeks of age can be seen in Figure 11.

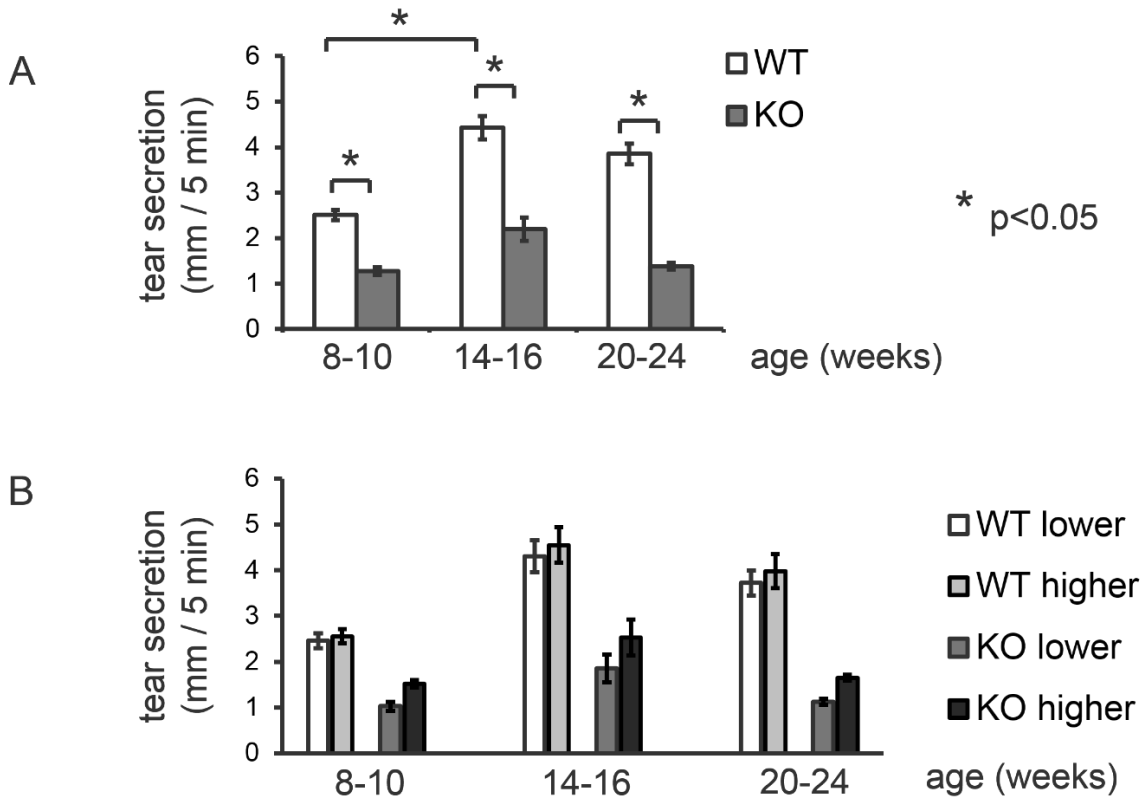

Figure 10. Tear secretions of WT and CFTR KO mice in 3 age groups.
A) Tear secretion was measured in three age groups: at 8-10 weeks of age (WT n=11; CFTR KO n=11), at 14-16 weeks of age (WT n=12; CFTR KO n=7) and at 20-24 weeks of age (WT n=11; CFTR KO n=10) both in WT and CFTR KO mice. Data from both eyes were averaged and evaluated. Tear secretion of CFTR KO mice were significantly lower compared to WTs in each age group. When tear secretion results of WT and CFTR KO mice were compared separately in different age groups, the secretion of WT mice measured at the age of 14-16 weeks was significantly higher compared to the 8-10 weeks group.
B) Secretion results of the eyes with the higher and the lower secretion were assessed and evaluated separately in WT and KO animals in each age group. Inter-ocular difference in tear secretion did not differ either in WT or in KO mice.

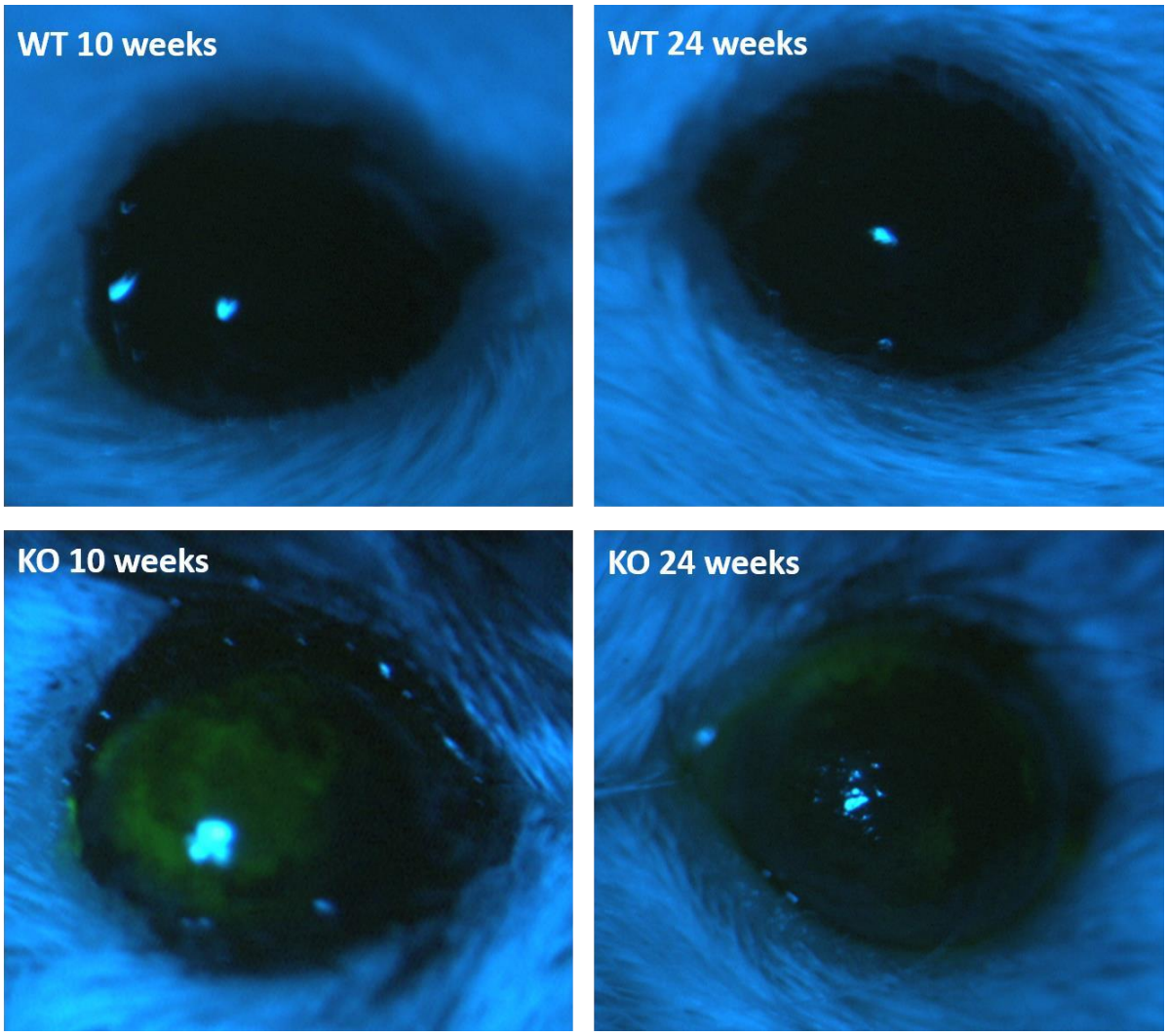

Figure 11. Evaluation of ocular surface integrity of WT and CFTR KO mice at 10 and 24 weeks. Virtually no fluorescence staining could be found in the corneas of WT mice, whereas profound staining were observed in the corneas from KO animals, in both age groups.

4.2.2. H&E staining of LGs from WT and CFTR KO mice

To assess the potential morphological differences between LGs from KO and WT mice, freshly dissected LGs were processed for H&E staining. LGs of 8-10 and 20-24 weeks old animals were investigated. However, no obvious structural changes have been observed in KO LG tissues as compared to their age-matched WT counterparts (Figure 12).

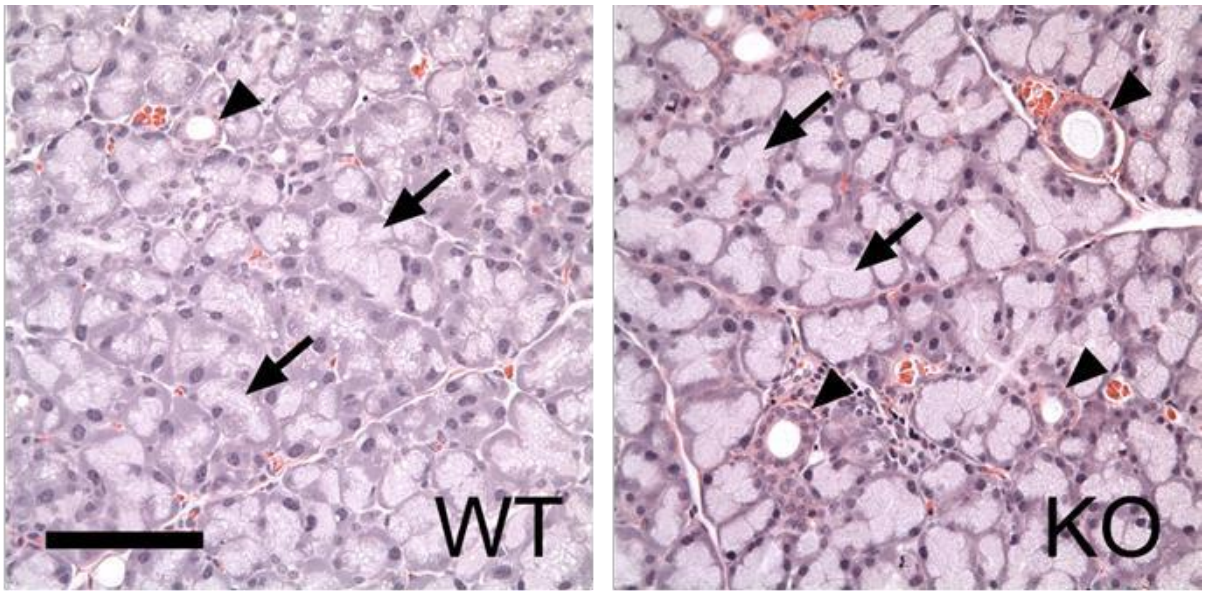

Figure 12. H&E staining of LG from WT and CFTR KO mice. While it appears that there are some increased luminal spaces within acinar cells (arrows) in WT mice, giving the image a less smooth appearance compared to that from KO mice, there are no significant morphological changes of the LGs, including ducts (arrowheads). Scale bar, 100 m.

4.2.3. Immunofluorescence staining for CFTR of WT and CFTR KO LGs

CFTR protein could be found in the apical membrane of LG duct cells deriving from WT animals. Strong staining was detected in the ducts whereas acinar cell membranes showed no signs of staining (Figure 13A-B). As anticipated, CFTR protein could not be identified in CFTR KO LGs (not shown).

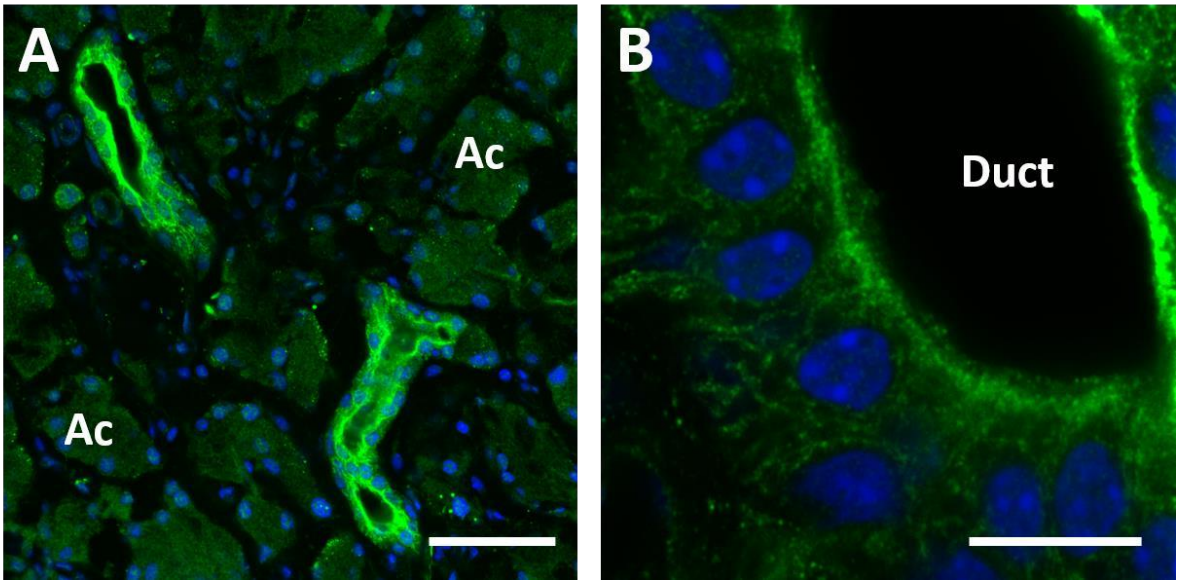

Figure 13. Immunofluorescence staining of CFTR in LGs from WT mice. CFTR staining was most prominent in the ducts (A and B), particularly in the apical membranes of the duct cells, while its presence in acinar cells (Ac) is diffusely distributed within the cytoplasm as punctate staining. Scale bar in A, 50 m; in B, 10 m.

4.2.4. Forskolin-induced fluid secretion of LG duct segments isolated from WT and CFTR KO mice

Effect of forskolin stimulation on WT and CFTR KO LG interlobular and intralobar duct segments isolated from 14-24 weeks old animals were investigated both in HEPES-buffered and in HCO_3^- buffered solutions. Ducts were superfused with HEPES-buffered solution for 10 min, and then 10 µmol/l forskolin was added to the bath. Forskolin stimulation resulted in a continuous, sustained swelling response in WT ducts (secretory rate: 181.5±6.1 pl/min/mm^2). In contrast, no forskolin-evoked fluid secretion could be measured in CFTR KO ducts (secretory rate: 1.1±5.6 pl/min/mm^2).

Using HCO_3^-/CO_2-buffered solution, forskolin stimulation resulted in a rapid secretion in WT ducts (secretory rate: 176.6±5.6 pl/min/mm^2). CFTR KO ducts remained unchanged with no secretory response observe during forskolin stimulation (secretory rate: 1.9±5.6 pl/min/mm^2). Figure 14A, 14B and 14C show the luminal volume changes for forskolin stimulation in WT and CFTR KO ducts.

Forskolin-induced fluid secretion was significantly lower in CFTR KO ducts compared to WTs (both in HEPES and in HCO_3^-/CO_2-buffered solutions: p=0.000). The secretory effect of forskolin in WT ducts did not differ significantly in HEPES-buffered and in HCO_3^-/CO_2-buffered solution (p=0.574).

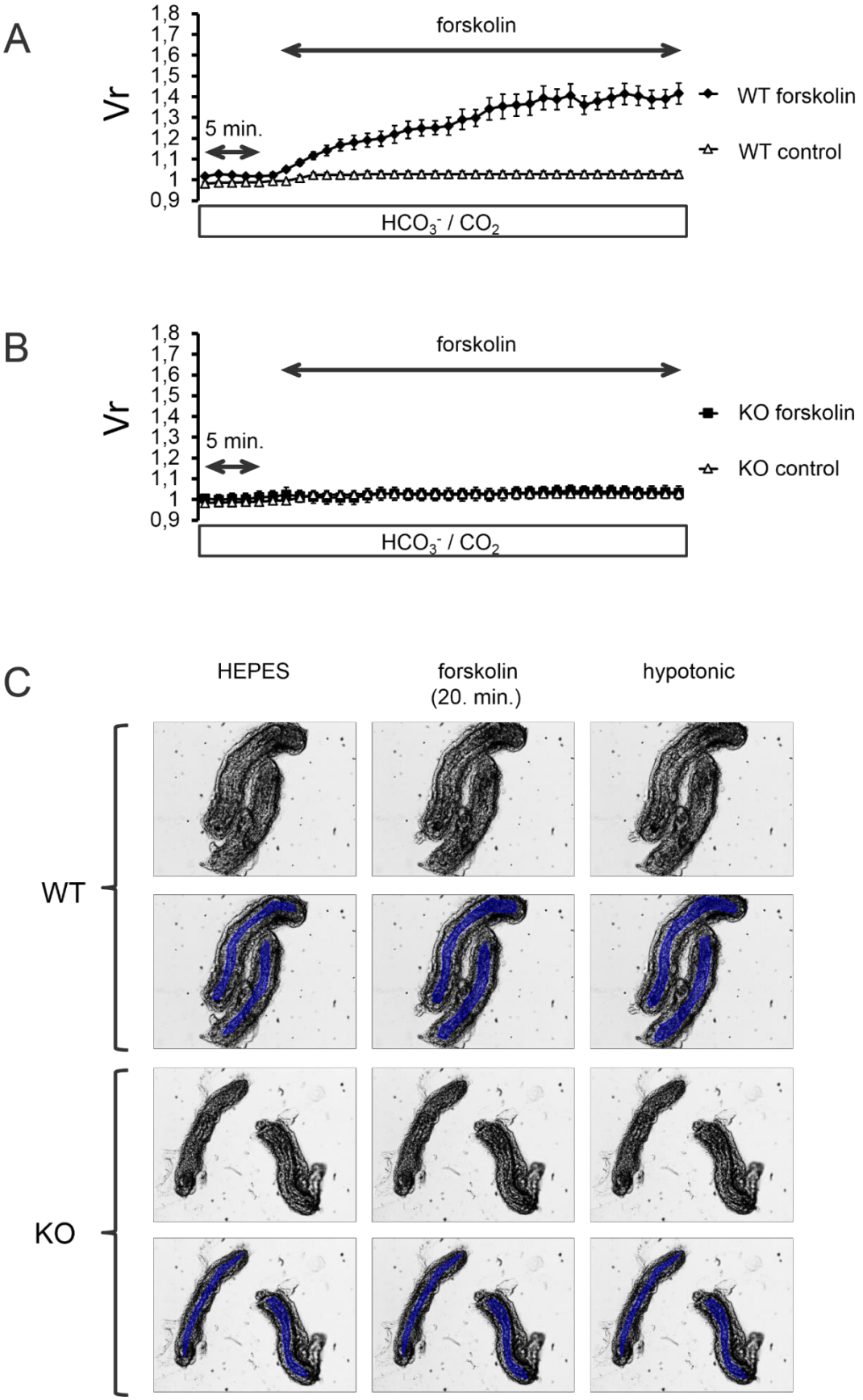
A
Vr
1,8
1,7
1,6
1,5
1,4
1,3
1,2
1,1
1
0,9
forskolin
5 min.
WT forskolin
WT control
HCO3- / CO2
B
Vr
forskolin
5 min.
KO forskolin
KO control
HCO3- / CO2
C
HEPES
forskolin
(20. min.)
hypotonic
WT
KO

Figure 14. Effect of forskolin on fluid secretion in mouse ducts isolated from WT and CFTR KO LGs. A) WT ducts were exposed either to 10 µM forskolin (filled rombus) or to no agonist (empty triangle). B) CFTR KO ducts were exposed either to 10 µM forskolin (filled square) or to no agonist (empty triangle). Changes in relative luminal volume (Vr) are shown. Data were obtained from six ducts isolated from three different animals in each series and are presented as means ± SEM. C) Photo series of secreting isolated LG duct segments in response to forskolin stimulation. The luminal space is marked with blue color.

5. DISCUSSION

Dry eye is the most common ocular surface disease affecting millions of people worldwide (33). Despite recent developments in the past few years, our treatment options are still limited, rendering the management of this debilitating disease very challenging (34, 35). Tear secretion is a complex process with the involvement of the main and accessory LGs, corneal and conjunctival epithelial cells and the Meibomian glands, etc. LG is the main source of fluid, electrolyte and proteins in the tear, and deficiency in its secretion results in aqueous deficient dry eye (6, 36). Our understanding of the physiological and pathological mechanisms of LG secretion is limited, despite its critical importance in developing new treatment strategies. More detailed understanding of LG function is therefore essential in order to develop novel approaches in the treatment of dry eye disease (9). Unfortunately, duct cells have been understudied for many years as compared to acinar cells, although recent advances clearly indicated that these duct cells play critical and indispensable roles in LG production (12, 13, 15, 37-39). Our laboratory is focusing on the clarification of the role of LG ducts in the secretory process of the gland. In the present work we aimed to investigate the main chloride transport systems of the ducts cells ie the NKCC1 on the basolateral (interstitial) membrane and the CFTR on the apical (luminal) side.

LG duct secretion is mediated by an array of ion transporters and channels including NKCC1, even though its role in LG duct secretion is not well understood. Remarkable differences in the expression of NKCC1 in the glandular epithelia of various species and organs can be observed. NKCC1 can be found in the basolateral membranes of rat and mouse pancreatic ducts, but not in the pancreatic and salivary gland duct cells of pig and guinea pig (17, 40, 41). Our present work evidenced the expression of NKCC1 in the basolateral membranes of both acinar and duct cells from rabbit LG by immunofluorescence with stronger staining observed in acinar cells. Investigations of various factors that may influence the activity of NKCC1 in LG duct cells were also performed.

It is widely accepted, that low intracellular Cl^- concentration can result in the activation of NKCC1 in many cell types (31, 32, 42). Activation of NKCC1 by low intracellular Cl^- level can facilitate Cl^- entry into the cell through the basolateral membrane to

restore cytosolic Cl^- homeostasis. Similarly to other investigated cells a significant increase in activity of NKCC1 was found in Cl^-- depleted LG duct cells in our present study.

NKCC1 plays a key role in volume regulation of cells, i.e., cell shrinkage can be a potent activation signal. The ability of NKCC1 to couple water and ion transport may play a direct role in the secretory process in epithelial cell (43, 44). Walcott and colleagues demonstrated the NKCC1-dependent manner of the regulatory volume increase in mouse LG acinar cells (16). In agreement with these previous findings hyperosmotic environment led to a marked increase of NKCC1 activity in rabbit LG duct cells.

Parasympathetic pathway in the activation of NKCC1 was also investigated in our study. We could not demonstrate notable effect of cholinergic agonist carbachol in the activation of NKCC1. This finding is in agreement with our previous results ie. cholinergic stimulation of isolated rabbit LG duct segments resulted in a very weak fluid secretory response. To further clarify the role of the cholinergic cellular signaling pathways, effects of Ca^{2+}-ionophore (A23187) and PKC activator PMA were measured. Elevation of cytosolic Ca^{2+} level with Ca^{2+} ionophore did not cause activation of NKCC1 in our experiments. In contrast, direct stimulation of PKC with its potent activator PMA resulted in a significant increase of NKCC1 activity, even though the rate of activation of the cotransporter was very weak. This contradiction between carbachol effect (no activation of NKCC1) and PMA effect (activation of NKCC1) might be explained by the weaker extent of activation of PKC during cholinergic effect compared to the direct and robust activation of the enzyme by PMA. Lack of effect of carbachol on NKCC1 might be explained also by the rapid cholinergic-evoked internalization of the cotransporter (45). This later effect could be a possible explanation by which carbachol and forskolin influence the activity of the cotransporter in different ways (45, 46). This theory is in agreement with our results, and explain, at least in part, the different fluid secretory patterns of Ca^{2+}- and cAMP-mediated mechanisms.

Besides acetylcholine, parasympathetic nerves also release VIP (8). Earlier reports demonstrated the presence of VIP receptors on acinar and duct cells of LG, thus we investigated the effects of VIP in the activation of NKCC1 (47). This transmitter acts predominantly through elevation of cytosolic cAMP level, the minority of its action thought

to be mediated by Ca^{2+} signaling. We could demonstrate a considerable increase of NKCC1 activity evoked by VIP stimulation.

Involvement of CFTR in the secretory process of various epithelial cells is widely investigated. Defective Cl^- and consequent fluid secretion can be observed in the pancreatic ducts, in the airways epithelium or in the salivary glands when CFTR protein is missing or aberrant (17, 37, 48-51). Unfortunately, little is known about the role CFTR may play in LG function, in contrast to the considerable attention paid to the other components of the ocular surface system, the cornea and the conjunctiva (52-54). CFTR was found to be expressed on the apical membrane of conjunctival and corneal epithelial cells (55-57). Levin and Verkman found high capacity for CFTR-facilitated Cl^- transport at the ocular surface in mice (58). In the present study, we demonstrated decreased tear secretion and increased corneal fluorescein staining in KO mice in all three age groups studied, as compared to age-matched WT mice, suggesting CFTR plays a critical and essential role in tear secretion and in the maintenance of ocular surface integrity. We also found significant increase in tear secretion in 14-16 weeks old WT mice, as compared to the 8-10 weeks old WT animals. This increase could not be observed in KO mice which may indicate the impaired reserve capacity of tear secretion during the examined life period in KO mice. Our results show that KO mice is a useful model to investigate the role of CFTR may play in LG secretion.

Histological examinations did not reveal any significant morphological differences between the WT and KO LG tissues either in the 8-10 weeks or in the 20-24 weeks old group. These histological results demonstrated that functional deterioration may precede morphological alterations during the course of disease progression. However, investigation of the duration of the disease in the alteration of LG morphology in CFTR KO mice has strong limitations as shorter life expectancies of CFTR KO mice hinder long lasting observations. Further studies are needed in order to clarify potential alterations in LG morphology later in life. In a case report by Alghadyan et al. histopathological examinations of LGs of CF patient who died of pulmonary complications revealed clogged small duct lumens and subsequent degeneration of acinar cells (59).

Our immunohistochemical examinations proved the strong predominance of CFTR protein in duct cells compared to the acini. Therefore to further elucidate the role of CFTR in LG function, we used LG duct segments isolated form WT and CFTR KO mice. This

experimental model suitable to study LG duct function was described earlier by our laboratory (12). Complete absence of forskolin-stimulated fluid secretion on video-microscopy observed in CFTR KO ducts represents the important role of CFTR may play in LG duct secretion in mice. Lack of cAMP-mediated fluid secretion in CFTR KO ducts demonstrates that CFTR can be the only cAMP-dependent transporter on the luminal surface of duct cells in mouse LG. In contrast with our finding of mouse LG ducts, pancreatic ducts isolated from CFTR KO mice has a considerable secretory capacity for forskolin stimulation (60). Considering the strong predominance of CFTR protein in LG ducts, CFTR could influence LG secretion through the modification of ductal secretion. Cl^- secretion through CFTR may be a major contributor to the transmembrane electrochemical gradient and subsequent electrolyte and water movements and therefore defects in CFTR may significantly compromise Cl^- and water secretion from LG ducts. In a recently published papers by Flores et al and Lee et al, small-molecule CFTR activators could increase tear secretion in a LG-ablated mouse model of dry eye (61, 62). Considering the lack of LG in this experimental model, source of enhanced Cl^- driven fluid secretion could be the conjunctival and corneal epithelial cells. Our present results provide evidence, that CFTR affects not only corneal and conjunctical epithelial cell function, but also LG secretion.

6. SUMMARY

In conclusion, our results presented here demonstrate the functional presence of NKCC1 in rabbit LG duct cells, providing further support that this transporter can be the main route of basolateral Cl^- uptake. We found that low cytosolic Cl^- level caused a significant increase in the activation of NKCC1. Hyperosmolarity of bath media, which results in cell shrinkage, proved to be a potent activator of NKCC1. NKCC1 could also be activated by elevated cytosolic cAMP level, VIP treatment and - in a considerably smaller extent – by direct activation of PKC. Our data demonstrated decreased tear secretion and impaired ocular surface integrity in CFTR KO mice, suggesting the important role of CFTR may play in LG function and in the maintenance of ocular surface integrity. We demonstrated strong predominance of CFTR protein in the duct cells compared to acinar cells. Our functional studies by employing our isolated duct segment model, suggest that CFTR plays a pivotal role in the fluid secretion of LG duct system. Further studies are needed to clarify whether modification of CFTR function may serve as a potential target to stimulate LG secretion and therefore can be an option in treating aqueous deficient dry eye.

Conclusions of the studies on LG ducts presented in the thesis are:

1) **NKCC1 is expressed on the basolateral membrane of the LG duct cells in rabbit**
2) **The transporter can be activated by low cytosolic Cl^- level, hyperosmolarity of bath media, elevated intracellular cAMP level, and in a smaller extent, by direct activation of PKC.**
3) **For the first time in LG research, CFTR KO mice were used to study the role of CFTR in ocular surface integrity and in the function of the LG.**
4) **CFTR KO mice exhibited considerably decreased tear secretion and increased corneal fluorescein staining compared to WTs, suggesting the pivotal role of CFTR in physiological tear secretion and in the maintenance of ocular surface health.**
5) **Strong predominance of CFTR protein was demonstrated on the basolateral membranes of duct cells compared to acinar cells in the LGs of WT mice.**

6) **Using our isolated duct segment model developed earlier, fluid secretion of LG ducts from WT and CFTR KO mice was investigated. Forskolin-induced elevation of cytosolic cAMP level resulted in strong secretory response in WT ducts, while no secretion was observed in KO ducts.**

Further researches are in progress in our laboratory in order to elucidate the role of various secretagouges in LG duct function in the presence and in the absence of CFTR protein. We are presently investigating the role of parasympathetic (ie. muscarinic agonist carbachol and VIP) and sympathetic stimuli in LG secretion. CFTR may influence and regulate other ion transporters located on the apical and the basolateral membranes of the epithelial cells, therefore the consequences of absent CFTR function in various ion transport processes of the LG duct epithelium have also to be clarified.

More detailed understanding of LG secretion at the cellular and molecular levels under physiological and pathological conditions is essential. Recent advances in our knowledge regarding the LG duct system, in addition to what we have known about the acinar cells, will likely promise new frontiers for researchers to develop novel approaches by targeting ductal cells to manage dry eye.

7. ACKNOWLEDGEMENTS

First of all I express my gratitude and appreciation to **Dr. Edit Tóth-Molnár** who introduced me to the experimental work and always helped and guided me during my PhD studies. Her attitude, inspiration and advices helped me to complete this work.

I am very grateful to **Professor András Varró** for giving me the opportunity to work in a highly inspiring scientific environment in the Department of Pharmacology and Pharmacotherapy.

I am indebted to **Professor Péter Hegyi** and **Professor Zoltán Rakonczay** for providing me all tools and instruments of the Pancreas Research Group needed in our experiments.

I wish to thank **Professor Andrea Facskó** for granting the necessary time for my experimental work.

I especially grateful to **Orsolya Berczeli**, **Dr. Máté Katona** and **all members of the Pancreas Research Group** for their continuous support and help during my entire work.

Last but not least I would like to express my sincere gratitude to **my parents** for their endless love and support in my all efforts.

The work was supported by the following grants:

NKFIH NN 115611 (Edit Tóth-Molnár)
EFOP-3.6.1-16-2016-00008 (Edit Tóth-Molnár)
The Webb Foundation Grant – Los Angeles (Chuanqing Ding & Edit Tóth-Molnár)
Momentum Grant of the Hungarian Academy of Sciences LP2014-10/2014 (Péter Hegyi)

8. REFERENCES

1. Craig JP, Nichols KK, Akpek EK. TFOS DEWS II Definition and Classification Report. *Ocul Surf.* 2017; 15: 278-283.

2. Hodges RR, Dartt DA. Tear film mucins: Front line defenders of the ocular surface; comparison with airway and gastrointestinal tract mucins. *Exp Eye Res.* 2013; 117:62-78

3. Willcox MDP, Argüeso P, Georgiev GA et al. TFOS DEWS II Tear Film Report. *Ocul Surf.* 2017; 15: 366-403.

4. Martin CL, Munnell J, Kaswan R. Normal ultrastructure and histochemical characteristics of canine lacrimal glands. *Am J Vet Res.*1988; 49:1566–1572.

5. Millar TJ, Herok G, Koutavas H, Martin DK, Anderton PJ. Immunohistochemical and histochemical characterisation of epithelial cells of rabbit lacrimal glands in tissue sections and cell cultures. *Tissue Cell Res*. 1996; 28:301–312.

6. Conrady CD, Joos ZP, Patel BCK. Review: The Lacrimal Gland and Its Role in Dry Eye. *Journal of Ophthalmology*. 2016; 2016:7542929. doi:10.1155/2016/7542929.

7. Dartt DA. Signal transduction and control of lacrimal gland protein secretion: a review. *Curr Eye Res.* 1989; 8(6):619-36.

8. Dartt DA. Neural regulation of lacrimal gland secretory processes: relevance in dry eye diseases. *Prog Retin Eye Res.* 2009; 28:155-177.

9. Alexander JH, vanLennep EW, Young JA. Water and electrolyte secretion by the exorbital lacrimal gland of the rat studied by micropuncture a nd cstheterization techniques. *Pflugers Arch.* 1972; 337:299-308.

10. Dartt DA. Moller M, Poulsen JH. Lacrimal gland electrolyte and water secretion in the rabbit: localization and role of (Na+/K+)-acivated ATP-ase. *J Physiol.* 1981; 321:557-569.

11. Ubels JL, Hoffman HM, Srikanth S, Resau JH, Webb CP. Gene expression in rat lacrimal gland duct cells collected using laser capture microdissection: evidence for K+ secretion by the duct cells. *Invest Ophthalmol Vis Sci.* 2006; 47:1876-1885.

12. Tóth-Molnár E, Venglovecz V, Ozsvári B el al. New experimental method to study acid/base transporters and their regulation in lacrimal gland ductal epithelia. Invest Ophthalmol Vis Sci. 2007; 48:3746-3755.

13. Katona M, Vizvari E, Nemeth L et al. Experimental evidence of fluid secretion of rabbit lacrimal gland duct epithelium. *Invest Ophthalmol Vis Sci*. 2014; 55:4360-4367.

14. Fernández-Salazar MP, Pascua P, Calvo JJ, *et al.* Basolateral anion transport mechanisms underlying fluid secretion by mouse, rat and guinea-pig pancreatic ducts. *J Physiol* 2004;556:415–28. doi:10.1113/jphysiol.2004.061762

15. Ding C, Parsa L, Nandoskar P, Zhao P, Wu K, Wang Y. Duct system of the rabbit lacrimal gland: structural characteristics and role in lacrimal sectretion. *Invest Ophthalmol Vis Sci.* 2010;51:2960-2967.

16. Walcott B, Birzgalis A, Moore LC, Brink PR. Fluid secretion and the Na+-K+-2Cl– cotransporter in mouse exorbital lacrimal gland. Am J Physiol Cell Physiol. 2005; 289: C860–C867.

17. Lee MG, Ohana E, Park HW, Yang D, Muallem S. Molecular mechanism of pancreatic and salivary gland fluid and HCO3- secretion. *Physiol Rev.* 2012; 92:39-74.

18. Hong JH, Park S, Shcheynikov N, Muallem S. Mechanism and synergism in epithelial fluid and electrolyte secretion. *Pflugers Arch.* 2014; 466:1487-1499.

19. Quinton PM. Physiological basis of cystic fibrosis: a historical perspective. *Physiol Rev.* 1999;79:S3–S22.

20. Reddy MM, Quinton PM. PKA mediates constitutive activation of CFTR in human sweat duct. *J Membr Biol.* 2009;231:65–78.

21. Steward MC, Ishiuro H. Molecular and cellular regulation of duct cell function. *Curr Opin Gastroenterol.* 2009; 25:447-53.

22. Roussa E. Channels and transporters in salivary glands. *Cell Tissue Res.* 2011;343(2):263-87.

23. Sheppard JD, Orenstein DM, Chao CC, Butala S, Kowalski RP. The ocular surface in cystic fibrosis. *Ophthalmology.* 1989; 96: 1624-30.

24. Castagna I, Roszkowska AM, Famà F, Sinicropi S, Ferreri G. The eye in cystic fibrosis. *Eur J Ophthalmol.* 2001; 11:9-14.

25. Mrugacz M, Kaczmarski M, Bakunowicz-Lazarczyk A, Zelazowska B, Wysocka J

Minarowska A. IL8 and IFN-gamma in tear fluid of patients with cystic fibrosis. *J Interferon Cytokine Res.* 2006; 26:71-5.

26. Lu M, Ding C. CFTR-mediated Cl^- transport in the acinar and duct cells of rabbit lacrimal gland. Curr Eye Res. 2012; 37(8):671-67.

27. Ratcliff R, Evans M J, Cuthbert AW, MacVinish LJ, Foster D, Anderson JR, Colledge WH. Production of a severe cystic fibrosis mutation in mice by gene targeting. *Nat Genet.* 1993; 4**:**35-41.

28. Seidler U, Singh A, Chen M et al. Knockout mouse models for intestinal electrolyte transporters and regulatory PDZ adaptors: new insights into cystic fibrosis, secretory diarrhoea and fructose-induced hypertension. *Exp Physiol* 2009; 94: 175-9.

29. Keiser NW, Engelhardt JF. New animal models of cystic fibrosis: what are they teaching us? *Curr Opin Pulm Med.* 2011; 17: 478-83.

30. Lemp MP: Report of the National Eye Institute: Industry Workshop on clinical trials in dry eyes. CLAO J. 1995; 21: 221-232.

31. Shumaker H, Soleimani M. CFTR upregulates the expression of the basolateral Na^+-K^+-$2Cl^-$ cotransporter in cultured pancreatic duct cells. *Am J Physiol Cell Physiol.* 1999; 277:C1100-C1110.

32. Heitzmann D, Warth R, Bleich M, Henger A, Nitschke R, Greger R. Regulation of the $Na^+2Cl^-K^+$ cotransporter in isolated rat colonic crypts. *Pflugers Arch-Eur J Physiol.* 2000; 439:378-384.

33. Stapleton F, Alvers M, Buny BY et al. TFOS DEWS Epidemiology Report. *Ocul Surf.* 2017; 15:334-365.

34. Milner MS, Beckman KA, Luchs JI et al. Dysfunctional tear syndrome: dry eye disease, and associated tear film disorders – new treatment strategies for diagnosis and treatment. *Curr Opinion Ophthalmol*. 2017; Suppl.1: 3-47.

35. Jones L, Downie LE, Korb D et al. TFOS DEWS II Management and Therapy Report. *Ocul Surf.* 2017; 15: 575-628.

36. Walcott B. The lacrimal gland and its veil of tears. *News Physiol Sci.* 1998; 13:97-103.

37. Nandoskar P, Wang Y, Wei R et al. Changes of chloride channels in the lacrimal glands of a rabbit model of Sjögren syndrome. *Cornea.* 2012; 31:273-279.

38. Ding C, Nandoskar P, Lu M, Thomas P, Trousdale MD, Wang Y. Changes of aquaporins in the lacrimal glands of a rabbit model of Sjögren's syndrome. *Curr Eye Res.* 2011; 36:571-578.

39. Ding C, Lu M, Huang J. Changes of the ocular surface and aquaporins in the lacrimal glands of rabbits during pregnancy. *Mol Vis.* 2011; 17:2847-2855.

40. Fernández-Salazar MP, Pascua P, Calvo JJ et al. Basolateral anion transport mechanisms underlying fluid secretion by mouse, rat and guinea-pig pancreatic ducts. *J Physiol.* 2004; 556:415-428.

41. Grotmol T, Buanes T, Raeder MG. N,N'-dicyclohexylcarbodimide (DCCD) reduces pancreatic NaHCO3 secretion without changing pancreatic tissue ATP levels. *Acta Physiol Scand*. 1986; 128:547-554.

42. Bachmann O, Wüchner K, Rossmann H et al. Expression and regulation of the Na^+-K^+-$2Cl^-$ cotransporter NKCC1 in the normal and CFTR-deficient murine colon. *J Physiol.* 2003; 549:525-536.

43. Hamann S, Herrera-Perez JJ, Bundgaard M, Alvarez-Leefmans FJ, ZeuthenT. Water permeability of Na^+-K^+-$2Cl^-$ cotransporters in mammalian epithelial cells. *J Physiol.* 2005; 568:123-135.

44. Hamann S, Herrera-Perez JJ, Zeuthen T, Alvarez-Leefmans FJ. Cotransport of water by Na^+-K^+-$2Cl^-$ NKCC1 in mammalian epithelial cells. *J Physiol.* 2010; 588:4089-4101.

45. Reynolds A, Parris A, Evans LA et al. Dynamic and different regulation of NKCC1 by calcium and cAMP in the native human colonic epithelium. *J Physiol.* 2007; 507-524.

46. Del Castillo IC, Fedor-Chaiken M, Song JC et al. Dynamic regulation of Na+-K+-2Cl- cotransporter surface expression by PKC in Cl- secretory epithelia. *Am J Physiol Cell Physiol.* 2005; 289:C1332-C1342.

47. Hodges R, Zoukhri D, Sergheraert C, Zieske JD, Dartt DA. Identification of vasoactive intestinal peptide receptor subtypes in the lacrimal gland and their signal-transducing components. *Invest Ophthalmol Vis Sci.* 1997; 38: 610-619.

48. Ishiguro H, Yamamoto A, Nakakuki M et al. Physiology and pathophysiology of bicarbonate secretion by pancreatic duct epithelium. *Nagoya J Med Sci.* 2012; 74:1-18.

49. Ohana E. Transepithelial ion transport across duct cells of the salivary gland. *Oral Dis.* 2015; 21:826-35.

50. Hollenhorst MI, Richter K, Fronius M. Ion transport by pulmonary epithelia. *J Biomed Biotechnol.* 2011; doi: 10.1155/2011/174306.

51. Saint-Criq V, Gray MA. Role of CFTR in epithelial physiology. *Cell Mol Life Sci.* 2017; 74:93-115.

52. Yu D, Thelin WR, Rogers TD, Stutts MJ, Randell SH, Grubb BR, Boucher RC. Regional differences in rat conjunctival ion transport activities. *Am J Physiol Cell Physiol.* 2012; 303(7): C767-80.

53. Holm K, Kessing SV. Conjunctival goblet cells in patients with cystic fibrosis. *Acta Ophthalmol*. 1975; 53:167–72.

54. Li J, Allen KT, Sun XC, Cui M, Bonanno JA. Dependence of cAMP mediated increase in Cl^- and HCO_3^- permeability o CFTR in bovine corneal endothelial cells. *Exp Eye Res.* 2008; 86: 684-90.

55. Turner HC, Bernstein A, Candia OA. Presence of CFTR in the conjunctival epithelium. *Curr Eye Res* 2002 Mar; 24(3):182–7.

56. Cao L, Zhang XD, Liu X, Chen TY, Zhao M. Chloride channels and transporters in human corneal epithelium. *Exp Eye Res.* 2010; 90: 771-9.

57. Sun XC, Bonanno JA. Expression, localization and functional evaluation of CFTR in bovine corneal endothelial cells. *Am J Physiol Cell Physiol*. 2002; 282: C672-C683.

58. Levin MH, Verkman AS. CFTR-regulated chloride transport at the ocular surface in living mice measured by potential differences. *Invest Ophthalmol Vis Sci*. 2005; 46: 1428-34.

59. Alghadyan A, Aljindan M, Alhumeidan A, Kazi G, McMhon R. The lacrimal glands in cystic fibrosis. *Saudi J Ophthalmol.* 2013; 27: 113-6.

60. Pascua P, Garcia M, Fernández-Salazar MP et al. Ducts isolated from the pancreas of CFTR-null mice secrete fluid. *Pflugers Arch.* 2009; 459:203-214.

61. Flores AM, Casey SD, Felix CM, Phuan PW, Verkman AS, Levin MH. Small-molecule CFTR activators increase tear secretion and prevent experimental dry eye disease. *FASEB J.* 2016; 30(5): 1789-97.

62. Lee S, Phuan PW, Felix CM, Tan JA, Levin MH, Verkman AS. Nanomolar-potency aminophenyl.1,3,5-triazine activators of the cystic fibrosis transmembrane conductance regulator (CFTR) chloride channel for prosecretory therapy of dry eye disease. *J Med Chem.* 2017; 60(3): 1210-1218.